

Motion Dynamics of a Rover With Slip-Based Traction Model

Kazuya Yoshida and Hiroshi Hamano
Tohoku University, Aoba 01, Sendai 980-8579, Japan
yoshida@astro.mech.tohoku.ac.jp

Abstract

This paper investigates kinetic behavior of a planetary rover with attention to tire-soil traction mechanics and articulated body dynamics, and thereby study the control when the rover travels over natural rough terrain. Experiments are carried out with a rover test bed to observe the physical phenomena of soils and to model the traction mechanics, using the tire slip ratio as a state variable. The relationship of load-traction factor versus the slip ratio is modeled theoretically then verified by experiments, as well as specific parameters to characterize the soil are identified. A dynamic simulation model is developed considering the characteristics of wheel actuators, the mechanics of tire-soil traction, and the articulated body dynamics of a suspension mechanism. Simulations are carried out to be compared with the corresponding experimental data and verified to represent the physical behavior of a rover.

1 Introduction

The effectiveness of a surface locomotion rover in planetary exploration has been proven by NASA's Pathfinder mission in 1997 [1] and, in upcoming missions, rovers are expected to traverse much longer distance over more challenging terrain, then achieve more complex tasks.

Corresponding to such growing attention, there are an increasing number of research papers being published to deal with technological issues on exploration rovers. The research area is very broad from mission design and analysis [3][4], rover designs [5][6][7], sensing and navigation, obstacle avoidance, path planning [8], motion kinematics and slip model [9], field test [10][11], and so on. However, very few have dealt with motion dynamics of rovers yet. This is because the rovers are, so far, considered to move too slowly to experience dynamic effect, and also the dynamic analysis requires complicated models and computation.

But recently, some papers report advantage of physics based motion control that involves a model of traction mechanics with the consideration of force distribution among the wheels [12][13][14][15]. In this approach the wheel-soil contact angle and the distribution of the load on each wheel were discussed, then an optimum control law that maximizes the traction and minimizes the power consumption was derived [9][15]. In these papers, ground

contact and force analysis were highlighted.

Extending the above approach, in the present paper, we investigate the tire-soil traction mechanics as well as the body-suspension-wheel dynamics of a rover. From the mission aspect, an exploration rover is discussed in Japan for a possible un-manned mission to the Moon [16], which will be jointly managed by NASDA (National Space Development Agency of Japan), ISAS (Institute of Space and Astronautical Science, Japan) and NAL (National Aerospace Laboratory of Japan.) On the lunar surface, terrain is composed mostly by fine grained soil (regolith) in which a rover may be easily stuck, and the gravity is smaller than a rover bounces more dynamically.

We therefore study the traction mechanics of a tire on loose soil, such as dry sand, and derive a model for *load-traction factor*, which is the ratio of the tangent and normal forces on a tire. Here, *slip ratio* of the tire is highlighted as a state variable, and the load-traction factor is derived as a function of the tire slip. The model is verified by experiments.

The motion dynamics of a rover is discussed with the model that a rover's suspension mechanism is treated as an articulated multi-body system connected by a free joint or a differential joint, or a spring-damper mechanism, if necessary. The motion of the rover is simulated using the driving force of the wheels as input.

This paper is organized as follows. In section 2, a rover test bed with 6 wheels connected by a Rocker-Bogie type link suspension is introduced. In section 3, the modeling of the rover is discussed for the tire-soil mechanics and the motion dynamics of the vehicle. In section 4, the model is verified by experiments. Characteristic parameters are identified, then the experimentally observed motion is examined by simulation.

2 Rover Test Bed

The rover test bed developed at Tohoku University, named "Nexus 6," has the dimension of within $0.4 \times 0.4 \times 0.4$ [m] cube and weighs 5.8 kg in total (see Figure 1.) It has 6 wheels connected by a Rocker-Bogie type suspension link system. Each wheel, in the diameter of 0.09 [m], is covered by soft rubber surface with small rubber spikes. Front and rear wheels have active steering DOF. The rocker-bogie is a non-spring suspension mechanism to connect wheels by free-pivot links. The mechanism

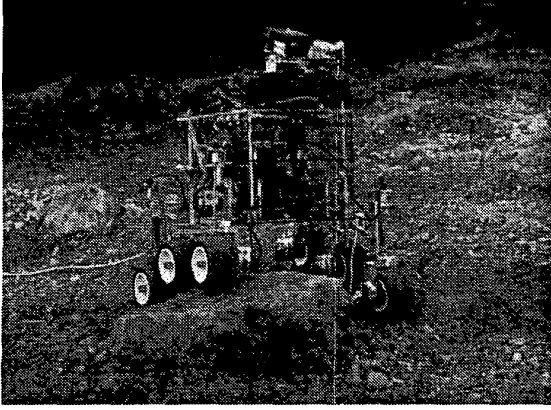


Figure 1: A rover test bed “Nexus 6” developed at Tohoku University

is known as one of successful suspension designs for the traversal capability on rough terrain [17]. The suspension mechanism of our test bed uses parallel links unlike that was used in the Pathfinder rover or other NASA’s recent Mars rover prototypes, but its functionality is almost the same. The right and left rocker links are connected by a differential mechanism.

In the main body, compact CPU boards (Hitachi H8) and motor drivers are mounted to control the driving torque of the wheels using pulse width modulation (PWM). The CPU cards communicate with a host computer through wired (RS-232C) or wireless (Ethernet) connection.

During the operation, duty ratio of the PWM pulse, which is effectively in proportion to the driving torque, is given to the motor driver of each wheel from the host computer as control input. The state of the rover is measured by following sensors: 6 tachogenerators for wheel angular velocity, 4 potentiometers for front and rear steering angles, 4 potentiometers for the suspension link angles (right and left rockers, right and left bogies.) The orientation and traveling velocity of the rover in the inertial frame is measured by a 3D video tracking system. For the tracking, 4 optical cue markers (colored balls) are attached on the test bed.

3 MODELING

3.1 Slip Ratio

As a key variable to describe the state of the rover, and to perform control, this paper focuses the slip ratio S of each wheel. It is defined as follows:

$$S = \begin{cases} (r\dot{\theta}_w - v_w)/r\dot{\theta}_w & (r\dot{\theta}_w > v_w : \text{accelerating}) \\ (r\dot{\theta}_w - v_w)/v_w & (r\dot{\theta}_w < v_w : \text{braking}) \end{cases} \quad (1)$$

where

- r : radius of the wheel
- θ_w : rotation angle of the wheel ($\dot{\theta}_w = \omega$)
- $r\dot{\theta}_w$: tire circumference velocity
- v_w : traveling velocity of the wheel

In this definition, the slip ratio is positive when the vehicle is accelerating and negative when braking.

3.2 Tire-Soil Interaction Mechanics

Figure 2 depicts a model of a wheel on deformable terrain. For such a model, a formula is known to describe the relationship between the share stress $\tau(\theta)$ and the normal stress $\sigma(\theta)$ of loose soil beneath the wheel [18]:

$$\tau(\theta) = (c + \sigma(\theta) \tan \phi)(1 - e^{a(S)}) \quad (2)$$

$$e^{a(S)} = -\frac{r}{k} \{ \theta_1 - \theta - (1 - S)(\sin \theta_1 - \sin \theta) \}$$

where

$$\tau_{max} = c + \sigma \tan \phi \quad (3)$$

represents a maximum share stress of the soil.

Also, another formula for the normal stress to relate the wheel’s vertical sinkage h has been proposed [19]:

$$\sigma(h) = (k_1 + k_2 b) \left(\frac{h}{b}\right)^n \quad (4)$$

where the geometrical relationship for h is:

$$h = r(1 - \cos \theta_1) \quad (5)$$

In the above equations, the symbols are:

- c : cohesion stress of the soil
- ϕ : internal friction angle of the soil
- b : wheel width
- n, k, k_1, k_2 : constants

By integrating σ and τ over the entire contact area, from θ_2 to θ_1 , we obtain the normal and tangential forces exerting on the wheel:

$$f_n = rb \left\{ \int_{\theta_2}^{\theta_1} \sigma(\theta) \cos \theta d\theta + \int_{\theta_2}^{\theta_1} \tau(\theta) \sin \theta d\theta \right\} \quad (6)$$

for the normal force that is balanced to the load W , and

$$f_t = rb \left\{ \int_{\theta_2}^{\theta_1} \tau(\theta) \cos \theta d\theta - \int_{\theta_2}^{\theta_1} \sigma(\theta) \sin \theta d\theta \right\} \quad (7)$$

for the tangential force that is called *drawbar pull*.

Here, we are interested in the drawbar pull as a function of the slip ratio. Since it is difficult to obtain a closed form solution of the above equations for the slip S , the plots are numerically obtained for the ratio of the traction force (drawbar pull) and normal force, i.e. $F(S) = f_t/f_n$, which is called *load-traction factor*.

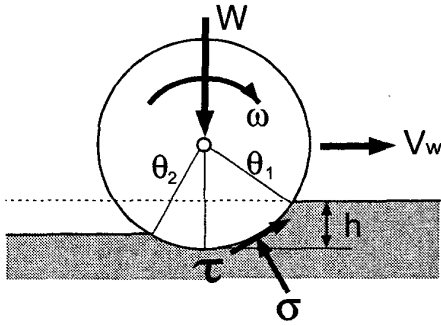


Figure 2: A tire model on deformable soil

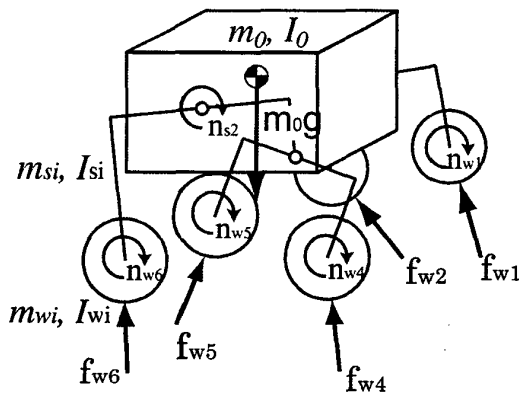


Figure 3: An articulated body model of the Rocker-Bogie suspension

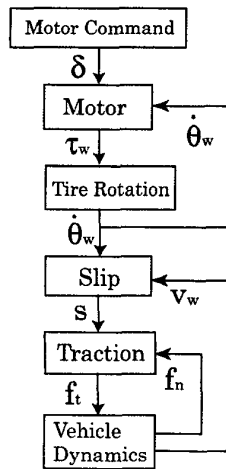


Figure 4: A computational flow for the forward dynamics simulation

3.3 Articulated Body Dynamics

Here, the motion dynamics of the rover is discussed with a model that the rover's suspension mechanism is treated as an articulated multi-body system. Figure 3 depicts the model representing forces and moments exerting on the system. Equation of motion for this system is formulated as follows:

$$H \begin{bmatrix} \dot{v}_0 \\ \dot{\omega}_0 \\ \dot{\theta}_s \\ \dot{\theta}_r \\ \dot{\theta}_w \end{bmatrix} + C = \begin{bmatrix} F_0 \\ N_0 \\ n_s \\ n_r \\ n_w \end{bmatrix} + J^T F_e \quad (8)$$

In this equation, the symbols are:

H : inertia matrix for the entire system composed by the inertia property of each body

C : non-linear velocity-dependent term

v_0 : translational velocity of the base body

ω_0 : rotational velocity of the base body

θ_s : suspension angle

θ_r : steering angle

θ_w : rotational angle of the wheel

$F_0 = (0, 0, -m_0g)^T$: forces exerting on the base body

N_0 : moments exerting on the base body

n_s : torque on the suspension joints

n_r : torque on the steering joints

n_w : driving torque of the wheels

J : Jacobian matrix

$F_e = (f_{w1}^T, \dots, f_{w6}^T)^T$: tire forces

Because of the differential mechanism between the right and left rocker links, there is a kinematic constraint so that $\theta_{s1} = -\theta_{s2}$ (angles are relative to the base body,) and the corresponding constraint torques are considered in N_0 and n_s .

The driving torque of the wheel is modeled including the characteristics of a PWM controlled DC motor. The tire force component f_{wi} is composed by the normal force f_{ni} and the tangential force f_{ti} . Given the sinkage and the slip ratio of each wheel, the normal stress and force are obtained from Equations (4) and (6), respectively. The tangential force is then obtained by multiplying the load-traction factor to the normal force.

3.4 Forward Dynamics Simulation

The authors have been developing an in-house software, in the form of MATLAB toolbox, for the numerical computations of kinematics and dynamics of articulated body systems. The toolbox is named *SpaceDyn* [20][21]. We

use it as a core module to obtain the forward dynamics solution of Equation (8).

The computational flow of the forward dynamics simulation is described in Figure 4. First, the PWM duty ratio δ is given as control input, then the motor torque is determined with the feedback of the back electromotive force that is a function of the angular velocity of the motor. Second, the slip ratio is evaluated from the velocities of the wheel and vehicle, then the traction forces are obtained using the load-traction factor. Finally, the vehicle dynamics is solved to obtain the acceleration of each part of the rover, then integrated to yield corresponding velocity and position.

The traveling velocity of the wheels is fed back to the slip evaluation. And also, by evaluating the interference of wheels with a surface geometry model, the wheel sinkage is evaluated to determine the normal forces.

By repeating this cycle, the motion of the rover is simulated in the virtual world.

4 Experimental Verification

In this section, the tire-soil contact model and the dynamics simulation model, discussed in the previous section, are verified by experiments. As for the tire-soil model, specific parameters to describe the load-traction factor are identified. For the dynamics model, the motion profiles are compared between the experiment and simulation.

Experiments are carried out for the rover to traverse over dry sand. The grain of the sand is almost between 0.2 and 2.0 millimeters. The test filed includes a sharp ditch in the depth of 5 centimeters and smooth slopes up to the inclination of 20 degrees. In order to test obstacle negotiation, several rocks with the diameter of 5-10 centimeters are scattered over the sand.

During the experiments, the angular velocity of each wheel and the angles of suspension links are measured on board. The velocity of the rover main body is measured external sensors, including a video tracking system. For the purpose of analysis, the traction force is evaluated from the angular velocity of the wheel using the characteristics of the corresponding motor. The normal load on each tire is evaluated from the body attitude and the suspension link angles considering static balance among forces and moments.

4.1 Identification of Tire-Soil Parameters

The load-traction factors for various slip ratios, observed in the experiments, are depicted in Figure 5. The data plots are relatively scattered, then mean values at each slip ratio are depicted with an error bar indicating $\pm 1SD$ (standard deviation.) It is observed that the plots show an increasing trend according to the slip ratio. The solid line in the figure shows a theoretical curve that makes a

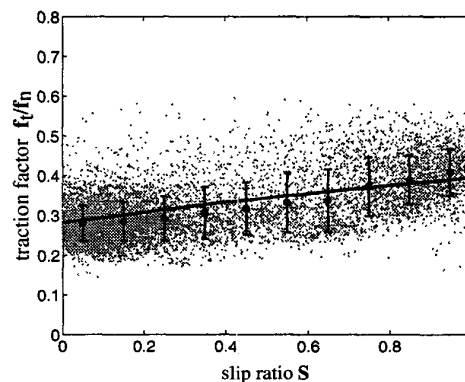


Figure 5: Traction factor v.s. slip ratio: experimental plots and a theoretical curve

Table 1. Characteristic parameters for the tire-soil interaction identified from experiments

c	0.005	[N/m ²]
ϕ	30	[deg]
k	0.05	[m]
θ_1	35.0	[deg]
θ_2	-5.0	[deg]

best fit with the experimental plots. To obtain the theoretical curve, the specific parameters are used in Equations (2)-(7) as listed in Table 1, where ϕ , c and k characterize the soil mechanics and may valid for most of dry sand. For example, in literature it appears that $\phi = 32$ [deg], $c = 0$ and $k = 0.025$ [m][18].

4.2 Verification of the Dynamics Simulation

Here, the results of the dynamics simulation are discussed by comparing with the experimental data.

Figure 6 shows a typical example for the rover to move over an obstacle. The figure compares the snap-shot motion of the rover and the rocker and bogie angles between the experiment and simulation. In the simulation, the same control command are given to the motors as the experiment. It appears that the time scale, which corresponds to the translational velocity of the rover, has difference between the two although, the overall profile shows good agreement. The simulation result well represents the performance of the rocker-bogie suspension system.

The reason of the difference may be inaccuracy of the surface model: i.e. in the simulation, all the surface is modeled as dry sand but, in reality, the obstacle has a hard surface while other flat area is composed by loose sand.

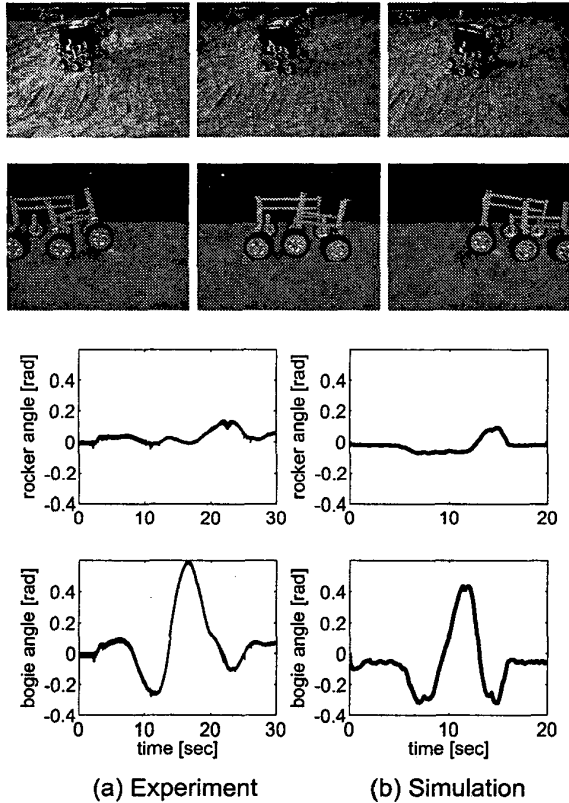


Figure 6: Rover motion moving over a bump: comparison of experiment and simulation

Figure 7 shows a case to negotiate with a slope that has an increasing inclination. In the experiment, the slip ratio stays near 0 before $t = 25$ [s], which means the tire grips the surface without slip. At $t = 25$ [s], the inclination of the slope reaches almost 12 degrees. After that the slip ratio increases up to 1, which means that the tire loses the grip. The elevation stayed constant after $t = 30$ [s] when the slip ratio reached to almost 1, yet the wheel was still driving. At this situation, the tire driving force exceeded the maximum share force of the soil, then the wheel started to dig a hole and sink in it, and finally the rover was stuck.

In the simulation, the time scale (traveling velocity) is again different although, the slip ratio switches from 0 to 1 at the inclination of 12 degrees, same as the experiment. In this sense, the simulation well represents the kinetic motion of a rover traversing over loose soil. However, the elevation keeps rising after switching the value of the slip, because the digging and sinking process is not modeled in the simulation, but Figure 5 suggests the traction force exists even at $S = 1$, which is correct as far as the tire force is lower than the maximum share force of the soil.

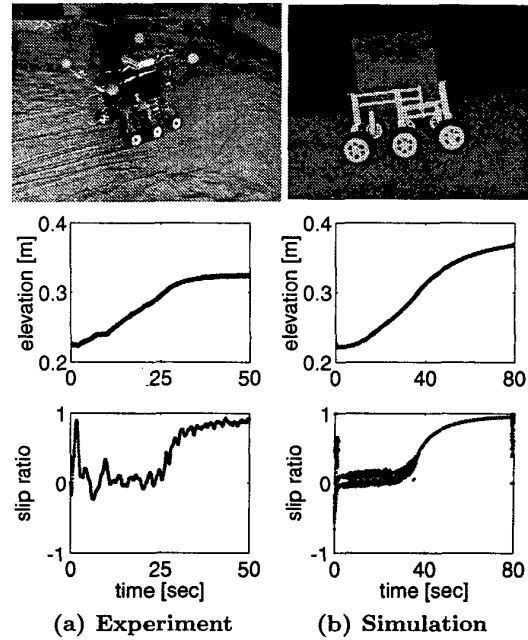


Figure 7: Rover motion to climb up a slope: comparison of experiment and simulation

5 Conclusions and Future Work

In this paper, the authors have investigated the kinetic behavior of a planetary rover with attention to tire-soil traction mechanics and articulated body dynamics, when the rover travels over natural rough terrain. They also have developed an effective control law to increase the traversability paying attention to the slip of the wheels.

Experiments were carried out with a rover test bed to observe the physical phenomena of soils and to model the traction mechanics using the tire slip ratio as a state variable. The relationship of load-traction factor versus the slip ratio has been modeled theoretically then verified by experiments. Specific parameters to characterize the soil have been also identified.

A dynamics simulation model was developed considering the characteristics of a wheel actuator, the mechanics of tire-soil traction, and the articulated body dynamics of a suspension mechanism. Simulations were carried out to compare the corresponding experimental data and verified to represent the physical behavior of the rover.

As a future research, the authors are interested in a control method that uses the slip ratio to keep it within a small value and limits excessive tire force, so that the rover can successfully traverse over an obstacle without digging the soil or being stuck.

The authors are also interested in simulating the rover

motion in the smaller gravity environment such as on the Moon or the Mars, where the dynamic effect will be much more highlighted.

Acknowledgements

A part of the experiments were carried out at the Robotics Laboratory in Tsukuba Space Center, NASDA, Japan. The research is supported by the Ministry of Education, Science, Sports and Culture, Grant-in-Aid for Scientific Research (B), 10044113, 1998-2001.

References

- [1] <http://mars.jpl.nasa.gov/MPF/> (as of Feb. 2002)
- [2] <http://mars.jpl.nasa.gov/mep/missions/announce2.html> (as of Feb. 2002)
- [3] C.R.Weisbin, D.Lavery, G.Rodriguez; "Robotics Technology for Planetary Missions Into the 21st Century," *Proc. i-SAIRAS'97*, Tokyo, Japan, July, 1997, pp.5-10.
- [4] C.R.Weisbin, et. al.; "Autonomous Rover Technology for Mars Sample Return," *Proc. i-SAIRAS'99*, ESTEC, The Netherlands, June, 1999, pp.1-10.
- [5] Paolo Fiorini; "Ground Mobility Systems for Planetary Exploration," *Proc. 2000 IEEE Int. Conf. of Robotics and Automation*, CA, USA, April, 2000, pp.908-913.
- [6] J.Aizawa, N.Yoshioka, M.Miyata, Y.Wakabayashi; "Designing of Lunar Rovers for High Work Performance," *Proc. i-SAIRAS'99*, ESTEC, The Netherlands, June, 1999, pp.63-68.
- [7] Y.Kuroda, K.Kondo, K.Nakamura, Y.Kunii, T.Kubota; "Low Power Mobility System for Micro Planetary Rover *Micro5*," *Proc. i-SAIRAS'99*, ESTEC, The Netherlands, June, 1999, pp.77-82.
- [8] M.Tarokh, Z.Shiller, S.Hayati; "A Comparison of Two Traversability Based Path Planners for Planetary Rovers," *Proc. i-SAIRAS'99*, ESTEC, The Netherlands, June, 1999, pp.151-157.
- [9] J. Balaram; "Kinematic Observers for Articulated Rovers," *Proc. 2000 IEEE Int. Conf. of Robotics and Automation*, CA, USA, April, 2000, pp.2597-2604.
- [10] S.Hayati, R.Arvidson; "Long Range Science Rover (Rocky7) Mojave Desert Field Tests," *Proc. i-SAIRAS'97*, Tokyo, Japan, July, 1997, pp.361-367.
- [11] W.R.Whittaker, D.Bapna, M.W.Maimone, E.Rollins; "Atacama Desert Trek: A Planetary Analog Field Experiment." *Proc. i-SAIRAS'97*, Tokyo, Japan, July, 1997, pp.355-360.
- [12] Farritor, S., Hacot, H., and Dubowsky, S.; "Physics-Based Planning for Planetary Exploration," *Proceedings of the 1998 IEEE International Conference on Robotics and Automation*: 278-283, 1998.
- [13] Iagnemma, K., Burn, R., Wilhelm, E., and Dubowsky, S.; "Experimental Validation of Physics-Based Planning and Control Algorithms for Planetary Robotic Rovers," *Proc. of the Sixth International Symposium on Experimental Robotics, ISER '99*, 1999.
- [14] Iagnemma, K., and Dubowsky, S.; "Vehicle Wheel-Ground Contact Angle Estimation: with Application to Mobile Robot Traction Control," *Proc. 7th International Symposium on Advances in Robot Kinematics, ARK 00*, 2000.
- [15] Iagnemma, K., and Dubowsky, S., "Mobile Robot Rough-Terrain Control (RTC) for Planetary Exploration," *Proceedings of the 26th ASME Biennial Mechanisms and Robotics Conference, DETC 2000*.
- [16] http://yyy.tksc.nasda.go.jp/sat/selene/index_e.html
<http://www.isas.ac.jp/e/enterp/missions/selene/> (as of Feb. 2002)
- [17] Bickler, D., "A New Family of JPL Planetary Surface Vehicles," *Missions, Technologies, and Design of Planetary Mobile Vehicles*, pp. 301-306, 1992.
- [18] Wong, J. Y., *Theory of Ground Vehicles*, John Wiley & Sons, 1978, chapter 2.
- [19] Bekker, G., *Introduction to Terrain-Vehicle Systems*, University of Michigan Press, 1969.
- [20] K. Yoshida; "The SpaceDyn: a MATLAB Toolbox for Space and Mobile Robots," *J. of Robotics and Mechatronics*, vol.12 no.4, pp.411-416, 2000.
- [21] <http://www.astro.mech.tohoku.ac.jp/spacedyn>